Cancer Cell
Article

Rb Regulates DNA Damage Response and Cellular Senescence through E2F-Dependent Suppression of N-Ras Isoprenylation

Awad Shamma,[1,2] Yujiro Takegami,[1] Takao Miki,[1,2] Shunsuke Kitajima,[1] Makoto Noda,[1] Takao Obara,[3] Takahiro Okamoto,[3] and Chiaki Takahashi[1,2,*]
[1]Department of Molecular Oncology
[2]The 21st Century Center of Excellence Formation
Kyoto University Graduate School of Medicine, Kyoto 606-8501, Japan
[3]Department of Endocrine Surgery, Tokyo Women's Medical University, Tokyo 166-8666, Japan
*Correspondence: chtakaha@virus.kyoto-u.ac.jp
DOI 10.1016/j.ccr.2009.03.001

SUMMARY

Oncogene-induced cellular senescence is well documented, but little is known about how infinite cell proliferation induced by loss of tumor suppressor genes is antagonized by cellular functions. *Rb* heterozygous mice generate *Rb*-deficient C cell adenomas that progress to adenocarcinomas following biallelic loss of *N-ras*. Here, we demonstrate that pRb inactivation induces aberrant expression of farnesyl diphosphate synthase, many prenyltransferases, and their upstream regulators sterol regulatory element-binding proteins (SREBPs) in an E2F-dependent manner, leading to enhanced isoprenylation and activation of N-Ras. Consequently, elevated N-Ras activity induces DNA damage response and p130-dependent cellular senescence in *Rb*-deficient cells. Furthermore, *Rb* heterozygous mice additionally lacking any of *Ink4a*, *Arf*, or *Suv39h1* generated C cell adenocarcinomas, suggesting that cellular senescence antagonizes *Rb*-deficient carcinogenesis.

INTRODUCTION

Carcinogenesis is induced by the breakdown of cellular functions that counteract various oncogenic stimuli (Hanahan and Weinberg, 2000). Oncogene-induced cellular senescence (OIS) was first noted as paradoxical growth arrest in human diploid fibroblasts induced by oncogenic Ras (Collado et al., 2007). Currently, OIS is accepted as the cellular function that antagonizes carcinogenesis despite the presence of oncogenic mutation. The study of melanocytic nevi carrying the $BRAF^{V600E}$ mutation provided the first evidence of cellular senescence in human premalignant lesions (Mooi and Peeper, 2006). Since then, the number of identified OIS inducers has been increasing rapidly (Di Micco et al., 2007).

OIS is achieved by activating tumor suppressors including $p16^{INK4a}$, ARF, pRB, and p53 or by inducing DNA damage response (DDR) activation engaged by γH2AX, Chk2, p53, and ATM before critical telomeric attrition occurs (Collado et al., 2007; Di Micco et al., 2007). These cellular functions counteract infinite cell proliferation induced by oncogenic signals. Accelerated cell proliferation induced by the loss of tumor suppressors can be counteracted by similar functions. For example, *PTEN* loss-induced prostate carcinogenesis is antagonized by p53-mediated senescence (Chen et al., 2005), and *VHL* loss-induced cellular senescence is mediated by pRB and p400 (Young et al., 2008). In human retinoblastoma, additional aberration in the p53 pathway is required for carcinogenesis (Laurie et al., 2006). Nevertheless, it is suspected that *RB* deficiency in the human body can be antagonized in many ways because of the diversified functions of pRB and the limited variety of mouse and human cell types that develop tumors with germline *RB* mutations (Wikenheiser-Brokamp, 2006).

SIGNIFICANCE

Aberration of the RB pathway critically pertains to human carcinogenesis. However, germline *RB* mutations are detected in a limited variety of malignant tumors, implicating the presence of defense mechanisms antagonizing *RB*-deficient tumorigenesis. In this study, we attempted to clarify the mechanism by which *N-ras* loci protect mouse C cells and primary fibroblasts from *Rb* loss-induced carcinogenesis and revealed a function of pRb in regulating posttranslational modification of CAAX proteins. Our findings explain the tumor suppressor function of N-Ras in certain types of cells lacking pRb. In addition, since Ras proteins promote carcinogenesis in many cell types, our findings may provide a rational basis for the application of prenyltransferase inhibitors to human cancers with aberrations in the RB pathway.

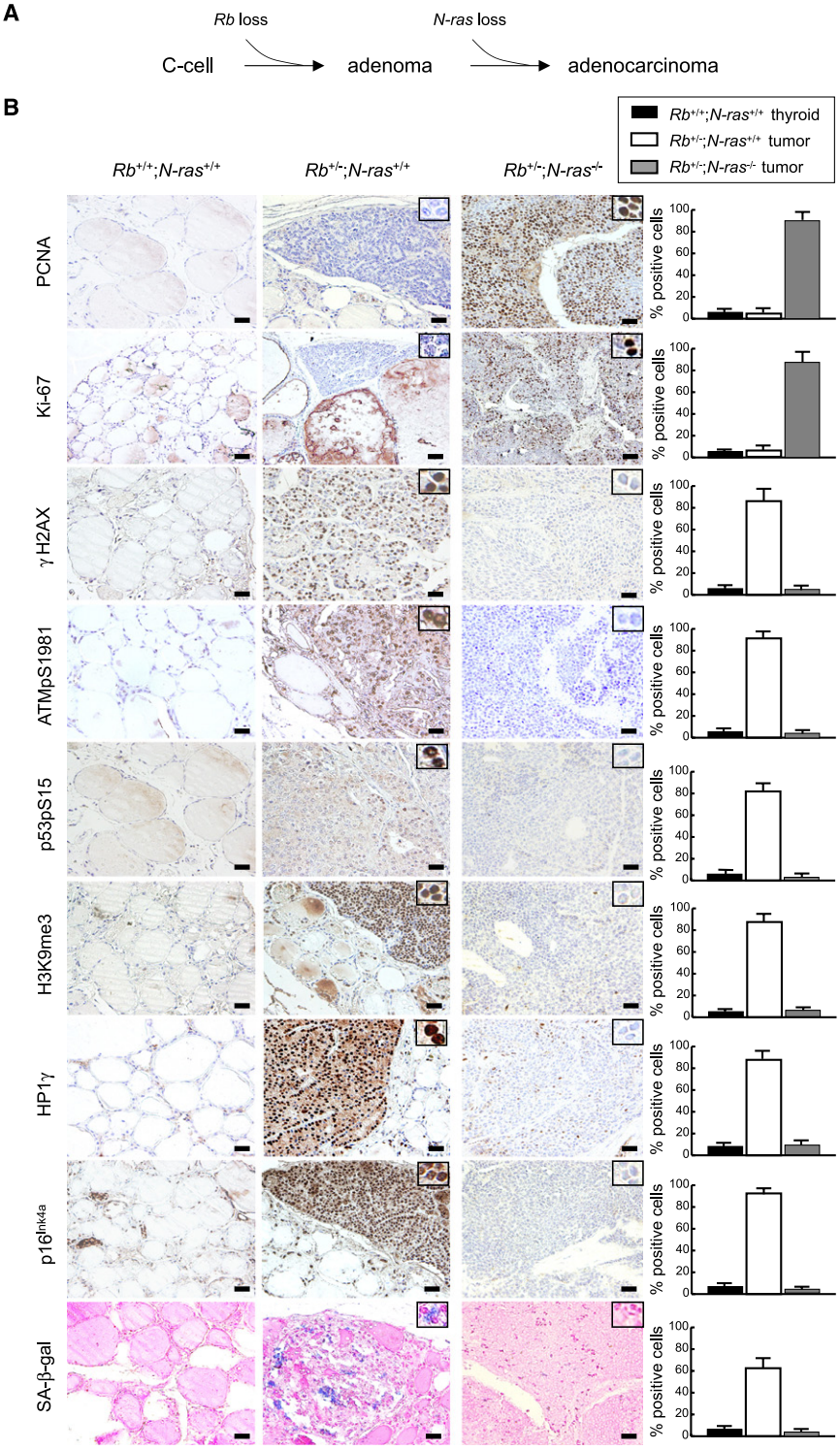

Figure 1. Analysis of C Cell Tumors in $Rb^{+/-}$;$N\text{-}ras^{+/+}$ and $Rb^{+/-}$;$N\text{-}ras^{-/-}$ Mice

(A) Scheme of C cell carcinogenesis in $Rb^{+/-}$ mice based on previous findings.

(B) Immunohistochemical (IHC) analysis and senescence-associated β-galactosidase (SA-β-gal) assay of thyroid and C cell tumors in mice of the indicated genotypes. Twenty-two $Rb^{+/-}$;$N\text{-}ras^{+/+}$ (average age at examination [AE] = 11.0 ± 1.2 months) and twenty-eight $Rb^{+/-}$;$N\text{-}ras^{-/-}$ (AE = 10.6 ± 0.9 months) mice were analyzed. Scale bars = 100 μm. The frequency of immunostain-positive cells per 200 normal thyroid or tumor cells is quantified at right. Bars show mean + SEM.

$Rb^{+/-}$ mice generate C cell adenoma in the thyroid following somatic loss of the normal *Rb* allele. Additional loss of *N-ras* alleles induces malignant conversion in *Rb*-deficient C cell adenoma. Moreover, somatic *N-ras* loss frequently occurs in $Rb^{+/-}$;$N\text{-}ras^{+/-}$ C cells following *Rb* loss, causing spontaneous malignant conversion (Takahashi et al., 2006). The C cell tumor phenotype observed in $Rb^{+/-}$;$E2F3^{-/-}$ mice (Ziebold et al., 2003) is similar to that in $Rb^{+/-}$;$N\text{-}ras^{-/-}$ mice. It has been proposed that the Rb-E2F complex functions as a transcriptional repressor to antagonize Ras signaling during vulval formation in *Caenorhabditis elegans* (Ceol and Horvitz, 2001). The *Rb-ras* genetic interaction during cell differentiation, embryogenesis, and tumorigenesis has been extensively investigated in mice (Lee et al., 1999; Takahashi et al., 2003, 2004, 2006); however, the core mechanism of this interaction has not yet been clarified. In this study, we sought in vitro and in vivo evidence that *Rb* loss-induced cell proliferation in mouse C cells and primary fibroblasts is counteracted by an N-Ras-dependent senescence pathway and attempted to elucidate the mechanism by which pRb regulates N-Ras activation.

RESULTS

N-ras-Dependent DDR and Cellular Senescence in *Rb*-Deficient C Cell Adenoma

To investigate how N-Ras prevents *Rb*-deficient C cell adenoma from progressing to adenocarcinoma (Figure 1A), we analyzed primary C cell tumors developed in $Rb^{+/-}$;$N\text{-}ras^{+/+}$ (average age at examination [AE] ± standard error of the mean [SEM] = 11.0 ± 1.2 months) and $Rb^{+/-}$;$N\text{-}ras^{-/-}$ (AE = 10.6 ± 0.9 months) mice. Proliferating cell nuclear antigen (PCNA) and Ki-67 were frequently expressed in *Rb*-deficient $N\text{-}ras^{-/-}$ adenocarcinomas, but their expression was invariably rare in *Rb*-deficient $N\text{-}ras^{+/+}$ adenomas (Figure 1B). On the other hand, *Rb*-deficient $N\text{-}ras^{+/+}$ adenomas frequently expressed DDR markers (Shiloh, 2003) including H2AX phosphorylated at serine 139 (γH2AX), ATM phosphorylated at serine 1981 (ATMpS1981), and p53 phosphorylated at serine 15 (p53pS15). These markers were rarely detected in $N\text{-}ras^{-/-}$ adenocarcinomas

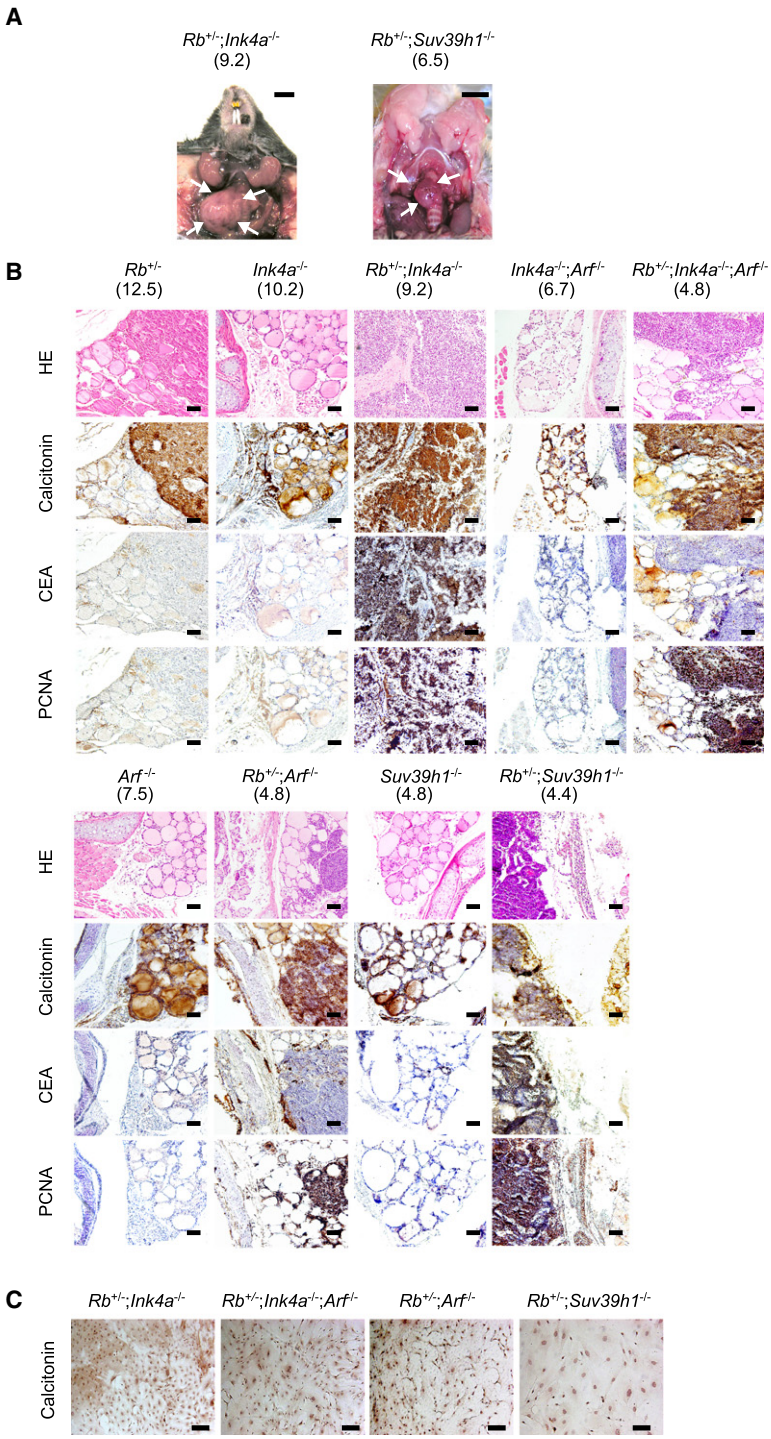

Figure 2. C Cell Tumor Phenotypes in *Rb*$^{+/-}$ Mice Additionally Lacking Senescence-Mediating Genes

(A) C cell tumors (indicated by arrows) developed in mice of the indicated genotype and age (months). Scale bars = 3 mm.

(B) Histological and IHC analysis of C cell tumors in mice of the indicated genotype and age (months). Scale bars = 100 μm.

(C) Calcitonin staining of cultured tumor cells prepared from thyroids of mice of the indicated genotype. Scale bars = 100 μm.

(Figure 1B). In addition, *N-ras*$^{+/+}$ tumors frequently expressed senescence markers (Dimri, 2005) including histone H3 trimethylated at lysine 9 (H3K9me3), heterochromatin protein 1γ (HP1γ), p16^{Ink4a}, and senescence-associated β-galactosidase (SA-β-gal) activity. These markers were rarely detected in *N-ras*$^{-/-}$ adenocarcinomas (Figure 1B) or in adenocarcinomas spontaneously developed in *Rb*$^{+/-}$;*N-ras*$^{+/-}$ mice as a consequence of somatic *N-ras* allele loss following *Rb* loss (see Figure S1 available online). These findings suggest that *N-ras* loci induce DDR and cellular senescence during adenoma formation initiated by *Rb* loss. We therefore hypothesized that N-Ras prevents *Rb*-deficient C cell adenomas from progressing to adenocarcinomas by inducing DDR and cellular senescence.

To determine the sequence of events during adenoma development, we compared *Rb*-deficient adenomas developed in younger *Rb*$^{+/-}$ mice (early adenoma; AE = 6.2 ± 0.3 months) to those in older mice (late adenoma; AE = 11.0 ± 1.2 months). DDR markers were expressed in early and late adenomas with similar frequencies; however, senescence markers were less frequently expressed in early adenomas (Figure S2). In contrast, PCNA and Ki-67 were more frequently expressed in early adenomas than in late adenomas. These findings suggest that DDR may precede cellular senescence during the development of C cell adenoma initiated by *Rb* loss, and that early adenomas grow even in the presence of DDR but cease to grow when cellular senescence is induced.

Role of Senescence-Mediating Genes in *Rb*-Deficient C Cell Adenoma

To examine whether cellular senescence protects *Rb*-deficient C cell adenomas from progressing to adenocarcinoma, we generated *Rb*$^{+/-}$ mice simultaneously lacking *Ink4a*, *Ink4a* and *Arf*, *Arf*, or *Suv39h1*. All *Rb*$^{+/-}$;*Ink4a*$^{-/-}$ mice survived longer than 8 months (n = 12). The average age at onset of sickness or death (ASD) was 9.3 ± 0.4 months in *Rb*$^{+/-}$;*Ink4a*$^{+/+}$ (n = 7), 9.5 ± 0.6 months in *Rb*$^{+/-}$;*Ink4a*$^{+/-}$ (n = 3), and 9.7 ± 0.4 months in *Rb*$^{+/-}$;*Ink4a*$^{-/-}$ (n = 6) mice. No acceleration of *Rb*-deficient pituitary tumorigenesis was observed in the *Ink4a*$^{-/-}$ background (data not shown). All *Rb*$^{+/-}$;*Ink4a*$^{-/-}$ mice exhibited large macroscopic tumors stemming from the thyroid (Figure 2A; Table 1). *Rb*$^{+/-}$;*Ink4a*$^{+/-}$ mice generated macroscopic tumors, but these were smaller than those in *Rb*$^{+/-}$;*Ink4a*$^{-/-}$ mice. No macroscopic thyroid tumors were observed in *Rb*$^{+/-}$;*Ink4a*$^{+/+}$ mice. Histologically, all thyroid tumors developed in *Rb*$^{+/-}$;*Ink4a*$^{-/-}$ and *Rb*$^{+/-}$;*Ink4a*$^{+/-}$ mice exhibited features of C cell adenocarcinoma (Figure 2B; Table 1) and were similar to tumors developed in *Rb*$^{+/-}$;*N-ras*$^{-/-}$ mice. *Rb*$^{+/+}$;*Ink4a*$^{-/-}$ mice showed no evidence of microscopic thyroid tumors. *Rb*-deficient *Ink4a*$^{-/-}$ cells separated from primary

Table 1. Pathological Diagnosis of Thyroids Derived from Mice of the Indicated Genotypes

Genotype	AE (months)	n	AD	CA	MD (mm)	CEA (%)	PCNA (%)	Ki-67 (%)
Rb$^{+/+}$;*Ink4a*$^{+/+}$	12.0 ± 1.0	5	0	0	–	–	–	–
Rb$^{+/-}$;*Ink4a*$^{+/+}$	9.8 ± 0.4	9	8	0	1.0 ± 0.2	1.4 ± 0.2	5.4 ± 0.4	4.6 ± 1.7
Rb$^{+/+}$;*Ink4a*$^{-/-}$	11.6 ± 0.4	3	0	0	–	–	–	–
Rb$^{+/-}$;*Ink4a*$^{+/-}$	10.0 ± 0.4	6	0	6	3.9 ± 0.2	66.3 ± 2.5	77.3 ± 2.0	74.7 ± 2.4
Rb$^{+/-}$;*Ink4a*$^{-/-}$	10.1 ± 0.3	8	0	8	8.6 ± 0.2	74.2 ± 2.0	84.2 ± 1.0	86.5 ± 1.8
Rb$^{+/-}$;*Arf*$^{+/+}$;*Ink4a*$^{+/+}$	6.2 ± 0.5	8	2	0	0.2 ± 0.1	NA	NA	NA
Rb$^{+/+}$;*Arf*$^{-/-}$;*Ink4a*$^{-/-}$	6.8 ± 0.1	5	0	0	–	–	–	–
Rb$^{+/-}$;*Arf*$^{+/-}$;*Ink4a*$^{+/-}$	7.3 ± 0.2	5	0	5	1.9 ± 0.2	2.5 ± 0.2	78.8 ± 1.5	76.9 ± 2.2
Rb$^{+/-}$;*Arf*$^{-/-}$;*Ink4a*$^{-/-}$	5.6 ± 0.3	6	0	6	3.5 ± 0.3	2.2 ± 0.3	82.4 ± 1.2	84.1 ± 1.6
Rb$^{+/-}$;*Arf*$^{+/+}$	5.4 ± 0.5	6	0	0	–	–	–	–
Rb$^{+/+}$;*Arf*$^{-/-}$	6.5 ± 1.0	6	0	0	–	–	–	–
Rb$^{+/-}$;*Arf*$^{+/-}$	6.5 ± 1.4	2	0	0	–	–	–	–
Rb$^{+/-}$;*Arf*$^{-/-}$	5.2 ± 0.3	5	0	5	1.7 ± 0.1	2.1 ± 0.2	57.8 ± 2.3	55.6 ± 2.2
Rb$^{+/-}$;*Suv39h1*$^{+/+}$	4.8 ± 0.3	6	0	0	–	–	–	–
Rb$^{+/+}$;*Suv39h1*$^{-/-}$	4.8 ± 0	2	0	0	–	–	–	–
Rb$^{+/-}$;*Suv39h1*$^{+/-}$	5.0 ± 0	3	0	0	–	–	–	–
Rb$^{+/-}$;*Suv39h1*$^{-/-}$	4.6 ± 0.2	8	0	8	3.6 ± 0.1	66.8 ± 2.3	81.1 ± 2.1	79.7 ± 2.3

Data shown include average age at examination (AE), number of analyzed thyroids (n), histological diagnosis of adenoma (AD) or carcinoma (CA), mean diameter of tumors (MD), and percentage of CEA-, PCNA-, and Ki-67-positive cells in tumors. Data are shown as ± SEM. –, no data; NA, not analyzed.

tumors grew in tissue culture and expressed calcitonin (5 successful cultures from 6 attempts with independent tumors) (Figure 2C), as did *Rb*-deficient *N-ras*$^{-/-}$ C cell adenocarcinoma cells. However, no clonally expanding calcitonin-positive cells were derived from thyroids harboring *Rb*-deficient *Ink4a*$^{+/+}$ tumors (0 of 6), suggesting that, like *Rb*-deficient *N-ras*$^{-/-}$ C cells, *Rb*-deficient *Ink4a*$^{-/-}$ C cell tumor cells had acquired the ability to infinitely proliferate. Therefore, we diagnosed tumors developed in *Rb*$^{+/-}$;*Ink4a*$^{-/-}$ mice as C cell adenocarcinomas. These findings suggest that C cell carcinogenesis initiated by *Rb* loss is blocked by *Ink4a*.

Rb$^{+/-}$;*Ink4a*$^{-/-}$;*Arf*$^{-/-}$ (ASD = 5.3 ± 0.1 months; n = 9) and *Rb*$^{+/-}$;*Arf*$^{-/-}$ (ASD = 4.7 ± 0.2 months; n = 3) mice died of lymphoma, sarcoma, or more often accelerated pituitary tumor growth as described previously (Tsai et al., 2002) before they developed macroscopic thyroid tumors. However, at 4.8 months, *Rb*$^{+/-}$;*Ink4a*$^{-/-}$;*Arf*$^{-/-}$ mice developed large microscopic adenocarcinomas with a morphology different from that of *Rb*-deficient *N-ras*$^{-/-}$ or *Rb*-deficient *Ink4a*$^{-/-}$ tumors (Figure 2B). *Rb*$^{+/+}$;*Ink4a*$^{-/-}$;*Arf*$^{-/-}$ mice of the same age or older showed no evidence of microscopic thyroid tumors (Table 1). In *Rb*$^{+/-}$;*Arf*$^{-/-}$ mice (AE = 5.2 ± 0.3 months), but not in *Rb*$^{+/+}$;*Arf*$^{-/-}$ mice, we often observed large microscopic adenocarcinomas with morphologies different from those in *Rb*-deficient *N-ras*$^{-/-}$, *Rb*-deficient *Ink4a*$^{-/-}$, or *Rb*-deficient *Ink4a*$^{-/-}$;*Arf*$^{-/-}$ tumors. Tumor cells separated from *Rb*$^{+/-}$;*Ink4a*$^{-/-}$;*Arf*$^{-/-}$ (3 of 3) and *Rb*$^{+/-}$;*Arf*$^{-/-}$ (2 of 2) mice grew in tissue culture and expressed calcitonin. However, in the *Arf*$^{-/-}$ background, regardless of *Ink4a* genotype and despite the frequent PCNA and Ki-67 expression and infinite growth in culture, the frequency of carcinoembryonic antigen (CEA)-positive C cell tumor cells was low (Figure 2B; Table 1). This suggests a specific genetic interaction between *Arf* and *CEA*. *Rb*$^{+/-}$;*Suv39h1*$^{-/-}$ mice (AE = 4.6 ± 0.2 months) exhibited macroscopic tumors (Figure 2A; Table 1) that grew in tissue culture (2 of 2) (Figure 2C) and frequently expressed CEA, PCNA, and Ki-67 (Figure 2B; Table 1). These findings suggest that *p16*^{Ink4a}, *Arf*, and *Suv39h1* antagonize *Rb*-deficient C cell carcinogenesis.

Role of N-Ras in *Rb*-Deficient C Cell Carcinogenesis

We generated 11 cell lines from independent primary *Rb*-deficient *N-ras*$^{-/-}$ thyroid tumors, all of which were calcitonin positive (data not shown). Six cell lines were less adhesive; five adhesive cell lines were competent for transfection and infection. After transduction of N-Ras or N-Ras^{V12}, all of the adhesive cell lines grew without immediate growth arrest or cell death for a minimum of 5 days. Moreover, upon subcutaneous inoculation into nude mice, one of the adhesive cell lines, AC61, produced tumors histologically similar to primary *Rb*-deficient *N-ras*$^{-/-}$ tumors. Importantly, this cell line generated smaller subcutaneous tumors with features of *Rb*-deficient adenomas when reconstituted with N-Ras at a level comparable to that of endogenous N-Ras expressed in the *Rb*-positive and *ret* mutation-positive human C cell adenocarcinoma cell line TT (Tomoda et al., 2008) (Figure 3A).

Nine days after *N-ras* transduction, we observed a marked induction of DDR (Figure 3B). Comet assay detected a high frequency of DNA double-strand breaks in N-Ras-transduced cells within 10 days (Figure 3C). At day 14, we observed marked induction of senescence markers, including recruitment of Suv39h1, H3K9me3, and HP1γ to the chromatin and induction of p16^{Ink4a}, p19^{Arf}, p107, and p130 (Figures 3D and 3E). We also detected senescence-associated heterochromatin foci (SAHF) (Narita et al., 2003) (Figure 3D) and high SA-β-gal activity (Figure 3F). The other four cell lines (AC55, 62, 65, and 69) responded to N-Ras in a manner similar to AC61 (Figure S3). We did not detect telomerase (mTERT) expression in AC61 cells. The AC55 cell line was telomerase positive; however, N-Ras

transduction did not significantly change mTERT expression or telomerase activity in AC55 cells, excluding the possibility of replicative senescence (Figures S4A–S4C). These findings indicate that in the absence of pRb, N-Ras induces DNA damage and cellular senescence, which functions as a barrier to C cell carcinogenesis.

p130-Dependent Differential Functions of Wild-Type and Oncogenic N-Ras in the Absence of pRb

When introduced into AC61 cells, N-Ras^{V12} was far less efficient at inducing DDR and senescence markers (Figures 3B–3E), growth arrest, and SA-β-gal activity (Figure 3F) compared to N-Ras. Furthermore, we observed only a slight decrease in the proliferation of pRb-reconstituted AC61 cells, suggesting that AC61 cells were reprogrammed to no longer be addicted to *Rb* loss (Figure 3F). The effects of N-Ras and N-Ras^{V12} in inducing cellular senescence were reversed after pRb reconstitution (Figure 3F). These findings suggest that pRb attenuates N-Ras function to induce cellular senescence in AC61 cells and that N-Ras^{V12} fails to activate alternative cellular senescence programs when pRb is unavailable.

We observed that p130 was markedly induced and accumulated in the nuclei of AC61 cells transduced with N-Ras, but not in AC61 cells transduced with N-Ras^{V12} (Figures 3E and 3G). Nuclear p130 was complexed with Suv39h1, H3K9me3, and HP1γ in the presence of N-Ras, but not N-Ras^{V12} (Figure 3G). Consistent with this, we detected the colocalization of p130 and HP1γ signals in the nuclei of N-Ras-reconstituted cells (Figure 3G). N-Ras failed to induce cellular senescence in AC61 cells when p130 was depleted beforehand by specific shRNAs (Figure 3H; Figure S5A). Moreover, p130 depletion at day 14 after N-Ras transduction significantly reversed cellular senescence (Figure 3I; Figure S5B). These findings suggest that p130 is required for induction and maintenance of N-Ras-induced cellular senescence in *Rb*-deficient cells. We also observed significant p130 induction in primary C cell adenomas developed in *Rb*$^{+/-}$;*N-ras*$^{+/+}$ mice, but not in adenocarcinomas developed in *Rb*$^{+/-}$;*N-ras*$^{-/-}$ mice (Figure 3J). Taken together, these findings suggest that induction of p130 is critical for cellular senescence induced by N-Ras in *Rb*-deficient C cell adenocarcinoma cells, and that N-Ras^{V12} fails to induce cellular senescence in these cells due to inability to induce p130.

Rb$^{-/-}$;*N-ras*$^{-/-}$ MEFs Escape Cellular Senescence

To generalize our observation on C cells, we characterized mouse embryo fibroblasts (MEFs) prepared from *Rb*$^{-/-}$ embryos with various *N-ras* genotypes. During the serial passages according to the 3T3 protocol (Todaro and Green, 1963), *Rb*$^{-/-}$;*N-ras*$^{-/-}$ MEFs achieved infinite proliferation significantly earlier than *Rb*$^{-/-}$ MEFs (Figure 4A). *Rb*$^{-/-}$;*Ink4a*$^{-/-}$ MEFs exhibited proliferative characteristics similar to those of *Rb*$^{-/-}$;*N-ras*$^{-/-}$ MEFs.

Rb$^{-/-}$;*N-ras*$^{-/-}$ MEFs, but not *Rb*$^{+/+}$;*N-ras*$^{+/+}$, *Rb*$^{-/-}$;*N-ras*$^{+/+}$, or *Rb*$^{+/+}$;*N-ras*$^{-/-}$ MEFs, could form colonies when plated at low cell density (Figure 4B). Moreover, shRNA-directed N-Ras depletion in *Rb*$^{-/-}$ MEFs allowed them to form colonies under the same conditions (Figure 4C). Furthermore, *Rb*$^{-/-}$;*Ink4a*$^{-/-}$ MEFs formed colonies when plated at low cell density, which was suppressed by p16^{INK4a}. Colony formation by *Rb*$^{-/-}$;*N-ras*$^{-/-}$ MEFs was suppressed by N-Ras, pRb, or p16^{INK4a}, but not by N-Ras^{V12} (Figure 4D). N-Ras^{N17} did not reduce colony numbers, suggesting that the function of N-Ras in colony suppression depends on GTP. The colony suppression in *Rb*$^{-/-}$;*N-ras*$^{-/-}$ MEFs induced by N-Ras was due to cellular senescence (Figure 4E; Figure S6). N-Ras^{V12} and other activated Ras isoforms did not induce cellular senescence but induced transformation in *Rb*$^{-/-}$;*N-ras*$^{-/-}$ MEFs (Figures 4E and 4F). However, N-Ras^{V12} induced senescence in *Rb*$^{+/+}$;*N-ras*$^{-/-}$ MEFs (Figure 4E) and wild-type MEFs (data not shown). A previous study demonstrated that *Rb*$^{-/-}$;*p107*$^{-/-}$;*p130*$^{-/-}$ MEFs escape cellular senescence and are efficiently transformed by H-Ras^{V12} (Sage et al., 2000). Similarly, *Rb*$^{-/-}$;*N-ras*$^{-/-}$ MEFs were transformed by all isoforms of Ras^{V12} (Figure 4F). These findings suggest that MEFs can be transformed by Ras^{V12} once exempted from the senescence program and thereby support the hypothesis that *Rb*$^{-/-}$;*N-ras*$^{-/-}$ MEFs escape cellular senescence.

Finally, to further elucidate the differential functions of N-Ras and N-Ras^{V12} in the absence of pRb, both proteins were simultaneously expressed in *Rb*$^{-/-}$;*N-ras*$^{-/-}$ MEFs. N-Ras was dominant over N-Ras^{V12} in inducing DDR and most of the senescence markers, but N-Ras^{V12} antagonized N-Ras activity to induce p16^{Ink4a} in the absence of *Rb* (Figure S6). These findings suggest that N-Ras and N-Ras^{V12} exert many different biological functions in the absence of *Rb*. To explain this difference, we analyzed their activation mechanisms in the studies discussed below.

pRb Attenuates N-Ras Activity in C Cell Adenocarcinoma

To address why N-Ras and N-Ras^{V12} exert different functions in the absence of pRb, we again analyzed AC61 cells. N-Ras expressed in AC61 cells was significantly activated; however, the activity was decreased to 10.4% (9.6 to 1.0) when pRb was simultaneously expressed under the influence of a strong promoter (Figure 5A). The relative activation level of N-Ras^{V12} (65.1) was 6.8 times higher than that of N-Ras (9.6) in the absence of pRb. The activity of N-Ras^{V12} was also attenuated by pRb, but this attenuation was less efficient (65.1 to 37.5) than that of N-Ras (9.6 to 1.0). Freshly introduced exogenous pRb was hyperphosphorylated when coexpressed with N-Ras^{V12} compared to N-Ras (Figure 5A), as expected from a previous study (Peeper et al., 1997). We therefore considered that hypophosphorylated pRb is more potent than hyperphosphorylated pRb in suppressing N-Ras activity. These findings suggest that in the absence of pRb, the activation level of N-Ras is moderate yet significantly lower than that of N-Ras^{V12}. This may at least partially explain the differential functions of N-Ras and N-Ras^{V12} in the absence of pRb.

pRb Delays N-Ras Isoprenylation

To explore the mechanism of N-Ras activation control by pRb, we transduced AC61 cells with moderately expressed pRb using a retrovirus of known titer (1.0 multiplicity of infection). We then transiently transduced these cells with the monomeric Venus^{A207R}-tagged N-Ras (Venus-N-Ras). The higher molecular weight endowed by tagging provided us with a better separation of proteins during SDS-PAGE. In addition, rapid analysis immediately after completing transfection and under optimal

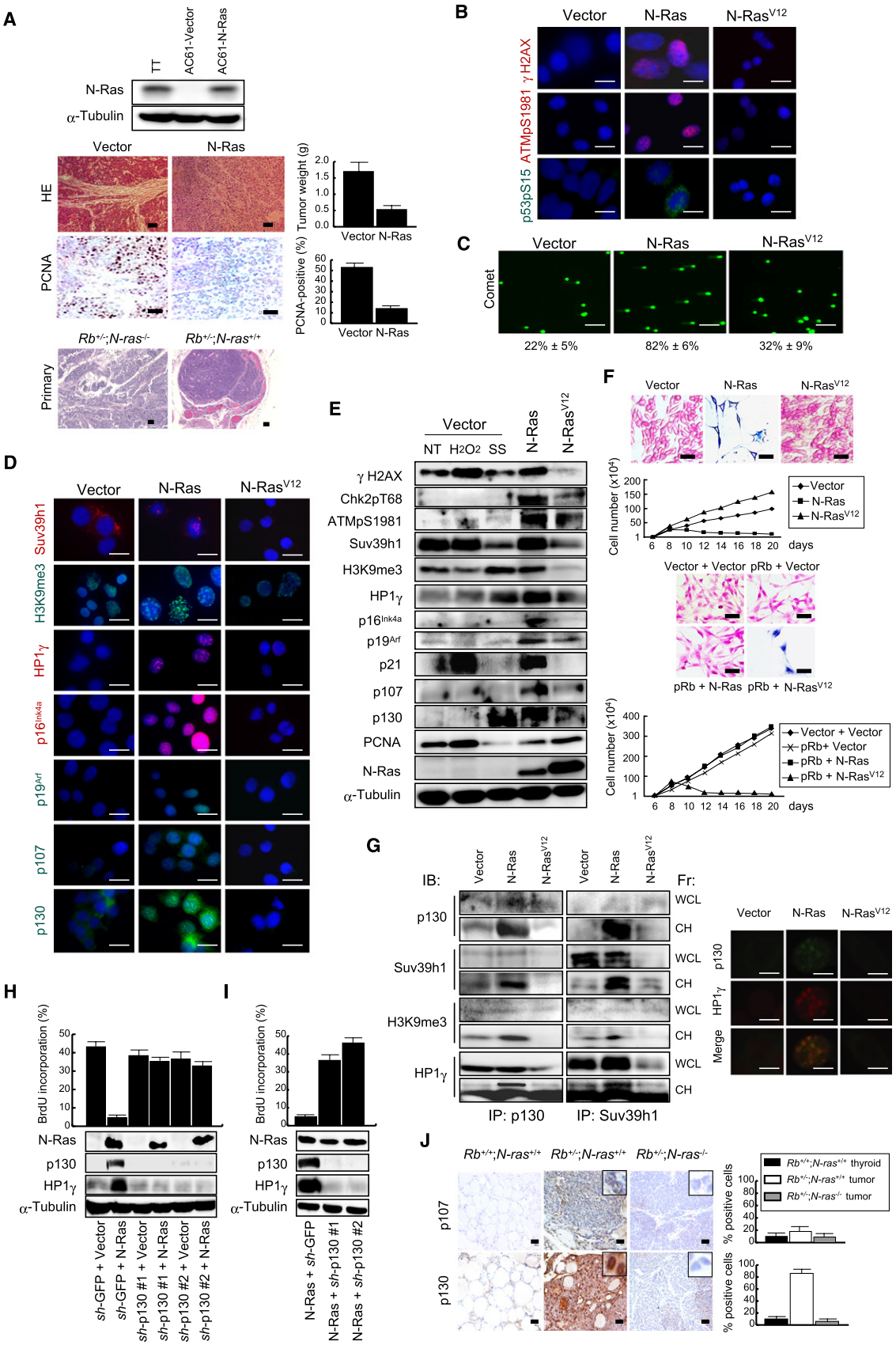
A
TT
AC61-Vector
AC61-N-Ras
N-Ras
α-Tubulin
Vector
N-Ras
HE
PCNA
Tumor weight (g)
Vector N-Ras
PCNA-positive (%)
Vector N-Ras
Rb+/-;N-ras-/-
Rb+/-;N-ras+/+
Primary
B
Vector
N-Ras
N-RasV12
γ H2AX
ATMpS1981
p53pS15
C
Vector
N-Ras
N-RasV12
Comet
22% ± 5%
82% ± 6%
32% ± 9%
D
Vector
N-Ras
N-RasV12
Suv39h1
H3K9me3
HP1γ
p16Ink4a
p19Arf
p107
p130
E
Vector
NT H2O2 SS
N-Ras
N-RasV12
γ H2AX
Chk2pT68
ATMpS1981
Suv39h1
H3K9me3
HP1γ
p16Ink4a
p19Arf
p21
p107
p130
PCNA
N-Ras
α-Tubulin
F
Vector
N-Ras
N-RasV12
Cell number (x10⁴)
days
Vector
N-Ras
N-RasV12
Vector + Vector
pRb + Vector
pRb + N-Ras
pRb + N-RasV12
Vector + Vector
pRb+ Vector
pRb + N-Ras
pRb + N-RasV12
G
IB:
Vector
N-Ras
N-RasV12
Vector
N-Ras
N-RasV12
Fr:
p130
WCL
CH
Suv39h1
WCL
CH
H3K9me3
WCL
CH
HP1γ
WCL
CH
IP: p130
IP: Suv39h1
Vector
N-Ras
N-RasV12
p130
HP1γ
Merge
H
BrdU incorporation (%)
N-Ras
p130
HP1γ
α-Tubulin
sh-GFP + Vector
sh-GFP + N-Ras
sh-p130 #1 + Vector
sh-p130 #1 + N-Ras
sh-p130 #2 + Vector
sh-p130 #2 + N-Ras
I
BrdU incorporation (%)
N-Ras
p130
HP1γ
α-Tubulin
N-Ras + sh-GFP
N-Ras + sh-p130 #1
N-Ras + sh-p130 #2
J
Rb+/+;N-ras+/+
Rb+/-;N-ras+/+
Rb+/-;N-ras-/-
p107
p130
% positive cells
Rb+/+;N-ras+/+ thyroid
Rb+/-;N-ras+/+ tumor
Rb+/-;N-ras-/- tumor

conditions enabled us to detect cytosolic (unprenylated) Venus-N-Ras proteins by immunoblotting (IB) and image analyses before the majority of these proteins became isoprenylated. In cells growing in 10% FBS, the moderate expression of pRb attenuated Venus-N-Ras activity to almost half (Figure 5B). However, under these conditions, the difference in the migration degree of Venus-N-Ras was barely noticeable. When we decreased FBS to 0.5% in an attempt to enhance pRb activity, we observed an increased proportion of the unprenylated form only in the presence of pRb. Under these conditions, the majority of pRb was hypophosphorylated. This effect of pRb was comparable to that of prenyltransferase inhibitors (PTIs) and was reversed by 1 hr serum restimulation. However, Venus-N-Ras activation upon serum restimulation was significantly delayed in the presence of pRb or PTIs (Figure 5B). We observed the same effect of pRb on N-Ras isoprenylation in another *Rb*-deficient *N-ras*$^{-/-}$ cell line (AC62) (Figure 5C). These findings suggest that pRb delays N-Ras isoprenylation and activation.

pRb Downregulates Membrane Trafficking of N-Ras

We observed an increased proportion of unprenylated N-Ras by IB in pRb-positive cells only when cultured under low serum conditions. N-Ras proteins in the isoprenylated fractions included not only those anchored to the plasma membrane but also those anchored to endomembranes such as Golgi, endoplasmic reticulum, and other vesicles. Thus, a considerable proportion of N-Ras is membrane anchored but not always activated. Therefore, we next investigated the effects of pRb on subcellular localization of N-Ras. We cotransfected Venus-N-Ras and red fluorescent protein (RFP)-tagged Rab6A (RFP-Rab6A) as a Golgi marker without the CAAX motif (Goud et al., 1990). Twelve hours after transfection in 10% FBS, Venus-N-Ras overlapping with RFP-Rab6A became detectable in both pRb-negative and -positive cells (Figure 5D). We then decreased the FBS concentration to 0.1% for 12 hr and observed that the signal overlap was barely detectable in pRb-positive cells, whereas it was readily detectable in pRb-negative cells. The abundance and subcellular localization of RFP-Rab6A were not affected by pRb or by serum depletion. PTIs exhibited the same effect as pRb during serum depletion. Under these conditions (0.1% FBS for 12 hr), we observed that in the absence of pRb, about half of the Venus-N-Ras was isoprenylated and enriched in the membrane fraction, whereas in the presence of pRb, most of the Venus-N-Ras was still unprenylated and remained in the cytosolic fraction (Figure 5D). After 18 hr serum depletion, we observed a slight recovery in the signal overlap in pRb-positive cells. Serum restimulation enabled the recovery of signal overlap to the initial level after 2 hr (Figure 5D). These findings suggest that serum concentration influences the pRb function in reducing N-Ras in Golgi at a particular time point. Disappearance of Venus-N-Ras from Golgi can be explained by downregulated transport to Golgi due to the decreased isoprenylation.

Next, to examine whether delayed membrane trafficking attenuates N-Ras activation, we observed AC61 cells cotransfected with Venus-N-Ras and RFP-Rab6A using a confocal laser microscope. After 24 hr culture in 10% FBS and subsequent 48 hr culture in 0.1% FBS, the overlap of Venus-N-Ras and RFP-Rab6A signals was significantly higher in pRb-negative cells than in pRb-positive cells; however, the Venus-N-Ras signal was not detectable at the plasma membrane in either (Figure 5E; Figure S7). Notably, 10 min after serum restimulation, a strong Venus-N-Ras signal was detected in the periphery of pRb-negative, but not pRb-positive, cells (Figure 5E; Figure S7). These observations suggest that pRb delays Venus-N-Ras transport to Golgi by attenuating endomembrane anchoring and thereby delays further trafficking to the plasma membrane. We further speculated that N-Ras-induced cellular senescence in *Rb*-deficient C cells depends on isoprenylation, as the N-Ras^{SAAX} (N-Ras^{S186}) mutant that cannot be isoprenylated completely failed to induce DDR and cellular senescence in AC61 cells (Figure 5F) or to suppress colony formation by *Rb*$^{-/-}$;*N-ras*$^{-/-}$ MEFs (data not shown). Similarly, treatment with PTIs significantly suppressed N-Ras-induced DDR and

Figure 3. Effects of N-Ras Reconstitution in *Rb*-Deficient *N-ras*$^{-/-}$ C Cell Adenocarcinoma

(A) Top: immunoblot (IB) analysis of TT and AC61 cells infected with pBabe-puro (vector) or pBabe-puro-N-Ras for the indicated proteins. Middle: histological and IHC analysis of AC61 cells infected with pBabe-puro or pBabe-puro-N-Ras, selected, and cultured subcutaneously in BALB/c-*nu/nu* mice for 14 days. Bottom: primary C cell tumors from mice of the indicated genotype. Scale bars = 100 μm. Right: quantification of tumor weights and frequency of immunostain-positive cells per 200 tumor cells. Bars show mean + SEM from n = 4 tumors each.

(B) Immunofluorescence (IF) analysis of AC61 cells infected with pBabe-puro vectors expressing the indicated proteins, selected, and cultured for additional 8 days. DAPI (blue) was used to visualize nuclei. Scale bars = 10 μm.

(C) Comet assay of cells in (B). Scale bars = 30 μm. Percentage of cells with DNA double-strand breaks is quantified below. Numbers show mean ± SEM from three experiments.

(D) IF analysis of cells prepared as in (B) and cultured for additional 12 days. Scale bars = 10 μm.

(E) IB of acid-extracted (γH2AX, Suv39h1, H3K9me3, and HP1γ) or whole-cell (others) lysates from cells prepared as in (B) and cultured for an additional 9 days. NT, nontreated; H_2O_2, treated with 200 μM H_2O_2 for 30 min at 4°C; SS, serum starved in 0.1% FBS for 24 hr.

(F) Top: AC61 cells were infected with pBabe-puro vectors expressing the indicated proteins and selected. Bottom: AC61 cells infected with pLXSB or pLXSB-Rb and selected were reinfected with pBabe-puro vectors expressing the indicated proteins and selected. Cell proliferation was monitored from day 6 onward, and SA-β-gal activity was detected at day 11 after the last infection. Scale bars = 30 μm.

(G) Left: immunoprecipitation (IP) from whole-cell lysates (WCL) or chromatin fraction (CH) of cells prepared as in (B) and cultured for additional 9 days. Upper bands show HP1γ bound to p130 or Suv39h1 in the chromatin fraction. Right: colocalization of p130 and HP1γ in these cells. Scale bars = 5 μm.

(H) AC61 cells were infected with lentiviruses expressing the indicated shRNAs and selected with puromycin. Five days after the initial infection, cells were reinfected with pLXSB or pLXSB-N-Ras, selected, and analyzed. BrdU incorporation as determined by fluorescence-activated cell sorting (FACS) and IB at day 6 after the last infection is shown. Bars show mean + SEM from duplicate experiments.

(I) AC61 cells were transduced with the indicated shRNAs 14 days after N-Ras transduction and analyzed as in (H). Bars show mean + SEM from duplicate experiments.

(J) IHC analysis of thyroids or primary C cell tumors in mice of the indicated genotypes. Scale bars = 100 μm. Quantification at right was performed as in Figure 1B. Bars show mean + SEM (n ≥ 20 each).

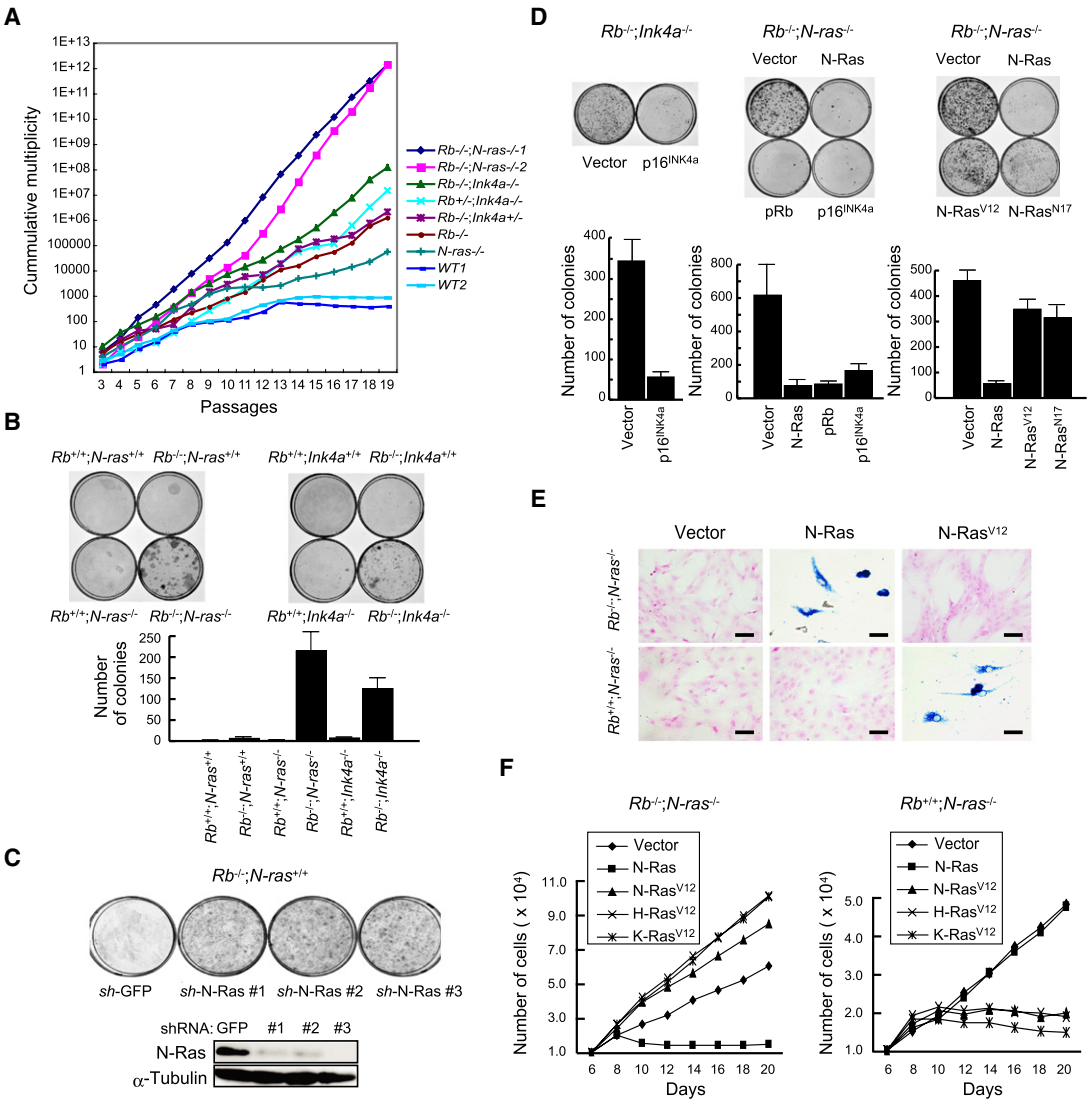

Figure 4. *Rb-N-ras* Genetic Interaction in MEFs

(A) 3T3 protocol assay of mouse embryonic fibroblasts (MEFs) of the indicated genotypes. Cumulative multiplicity in representative cultures at the indicated passage number is shown.

(B) Representative results of colony formation assays of MEFs of the indicated genotypes plated at low density. Results are quantified below. Bars show mean + SEM (n = 6).

(C) Top: $Rb^{-/-}$ MEFs infected with lentiviruses expressing the indicated shRNAs, selected, plated at low density, reinfected every 5 days three times, and cultured for 21 days from the initial infection. Bottom: IB analysis of cells infected once with the indicated lentiviruses.

(D) Colony suppression assay of MEFs of the indicated genotypes cotransfected with pLXSB and pBabe-puro vectors expressing the indicated proteins and selected. Bars show mean + SEM (n = 4).

(E) SA-β-gal assay of MEFs of the indicated genotypes infected with pBabe-puro vectors expressing the indicated proteins, selected, and cultured for 9 days. Scale bars = 100 μm.

(F) Proliferation of MEFs of the indicated genotypes infected with pBabe-puro vectors expressing the indicated proteins or pMIKcys (K-Ras^{V12}). After selection, 1×10^5 viable cells were plated on 100 mm dishes (day 6), and cell number was counted at the indicated time points.

cellular senescence in AC61 cells (Figure 5G). Finally, we examined whether *Rb* loss increases N-Ras isoprenylation. Venus-N-Ras was introduced into $Rb^{+/+}$ and $Rb^{-/-}$ MEFs. Upon serum starvation initiated 8 hr after transfection, $Rb^{-/-}$ MEFs exhibited faster isoprenylation of Venus-N-Ras protein compared to littermate $Rb^{+/+}$ MEFs (Figure 5H; Figure S8), suggesting that *Rb* loss in MEFs accelerates N-Ras isoprenylation.

pRb Downregulates Genes Involved in Isoprenylation

A previous study demonstrated that the influence of pRb on Ras activity depends on de novo protein synthesis (Lee et al., 1999). We therefore performed microarray analysis on AC61 cells freshly transduced with moderately expressed pRb. These cells were maintained unsynchronized in 10% FBS, which allowed the cells to attenuate N-Ras activity to half (Figure 5B). Genes

significantly upregulated by pRb included many cell surface antigens, lymphokines, interferons, and inflammation-related genes (Figure S9), similar to previous results obtained by analyzing MEFs conditionally lacking pRb (Markey et al., 2007). Moreover, in genes significantly downregulated by pRb, we detected known E2F targets such as *Cdc6*, *N-myc*, and *Mmp-3* with the highest statistical significance (change p value > 0.99998 as determined by Wilcoxon's signed rank test), suggesting that pRb reconstitution was successful (Table S1).

In 396 significantly upregulated genes (change p value < 0.001), we did not detect genes that could be directly involved in suppressing Ras activity such as GTPase-activating protein (*Gap*). In 270 significantly downregulated genes (change p value > 0.9998), we found that farnesyl diphosphate farnesyltransferase 1 (*Fdft1*) had the highest rank (Table S1). In addition, we detected a number of genes (Table S2) predicted to be transactivated by sterol regulatory element-binding proteins (SREBPs) via sterol regulatory element (SRE) (Sakakura et al., 2001). Other genes that could be directly involved in stimulating Ras activation, such as GTP exchange factor (*Gef*) or receptor tyrosine kinase (*Rtk*), were not detected. We then analyzed pRb-reconstituted AC61 cells by RT-PCR. Surprisingly, in addition to *Fdft1*, farnesyl diphosphate synthase (*Fdps*) (Szkopinska and Plochocka, 2005), most of the prenyltransferases (farnesyltransferase α [*Fnta*], farnesyltransferase β [*Fntb*], protein geranylgeranyltransferase 1β [*Pggt1b*], and Rab geranylgeranyltransferase β [*Rabggtb*]) (Maurer-Stroh et al., 2003), and *SREBP-1* and *SREBP-2* were significantly downregulated by pRb. All of these genes were induced in MEFs following *Rb* loss or pRb inactivation using SV40 large T antigen or adenovirus E1A (Figure 6A). A farnesyltransferase β immunoblot validated the RT-PCR results (Figure 6B). We did not detect a significant change in expression of *NF1* (Courtois-Cox et al., 2006) (data not shown).

To investigate the in vivo relevance of the increased expression of genes involved in protein isoprenylation in *Rb*-deficient cells, primary *Rb*-deficient C cell adenomas were immunohistochemically analyzed. These tumors expressed significantly higher levels of Fntb, SREBP-1, and SREBP-2 compared to normal thyroid tissue (Figure 6C). We then compared the expression levels of these proteins between pRb-positive *ret* mutation-positive human medullary thyroid carcinoma cell line TT (Tomoda et al., 2008) and AC61. AC61 cells expressed significantly higher levels of Fnta, Fntb, SREBP-1, and SREBP-2 compared to TT cells (Figure S10).

E2F-Dependent Transcription Control of Genes Involved in Isoprenylation

To further investigate the mechanism by which pRb controls genes involved in protein isoprenylation, we analyzed the promoter regions of these genes. We detected several E2F-binding consensus sequences in the promoter regions of *SREBP*s (Figure S11). Moreover, we detected several E2F-binding consensus sequences in each of the promoters of *Fdps* and prenyltransferases. These findings suggest that E2Fs control *Fdps* and prenyltransferases via a dual mechanism involving SREBPs and direct binding. Chromatin immunoprecipitation (ChIP) assay detected the direct binding of E2F-1 and E2F-3 to the promoters of these genes specifically in the absence of pRb (Figure 6D). E2F-3 exhibited stronger DNA-binding activity to the *Fntb* promoter than E2F-1 did. We also detected direct binding of pRb to the *Fdps* promoter. pRb prevented SREBPs from binding to the *Fdps* promoter, probably via downregulation of *SREBP*s. Furthermore, a pRb mutant derived from a retinoblastoma and lacking the ability to attenuate Ras activation (Lee et al., 1999) could not bind to the *Fdps* promoter and did not suppress SREBP binding. However, a partially penetrant mutant pRb (Sellers et al., 1998) with the ability to attenuate Ras activation (Lee et al., 1999) bound to the *Fdps* promoter and suppressed SREBP binding (Figure S12), suggesting that the function of pRb in attenuating Ras activation is not separable from its ability to regulate the *Fdps* promoter and SREBPs.

Fdps, *Fntb*, and *SREBP-1* promoters were downregulated by pRb. This effect was augmented by serum depletion. These promoters were upregulated by either E2F-1 or E2F-3 (Figure 6E). In particular, E2F-3 was more potent than E2F-1 in transactivating the *Fntb* promoter, in agreement with the ChIP results (Figure 6D). The truncated mutant E2F containing the DNA-binding domain but lacking the transactivation domain (E2F-DB) slightly but significantly downregulated these promoters, suggesting the involvement of liberated E2Fs in the basal transactivation. *Fdps* and *SREBP-1* promoters were upregulated by SREBP-1c, but the *Fntb* promoter, which lacks SRE, was not. The dominant-negative SREBP-1c downregulated the basal transactivation of these two promoters, indicating increased endogenous SREBP activity in AC61 cells. Furthermore, these three promoters were downregulated by pRb in two other pRb-negative cell lines ($Rb^{-/-}$;$N\text{-}ras^{-/-}$ MEFs and Saos2). Transduction of E2F-DB, SV40 large T antigen, or adenovirus E1A in MEFs induced *Fdps* promoter transactivation (Figure 6E). E2F-DB is known to affect the functions of E2Fs in multiple ways; one is derepression of active transcriptional silencing by the pRb-E2F complex (Rowland et al., 2002). Thus, we considered that the pRb-E2F complex directly participates in the transcriptional repression of *Fdps*.

pRb-Dependent Protein Farnesylation

The CAAX motif constitutes a C-terminal tetrapeptide common to all Ras proteins, directing multistep posttranslational modifications initiated by farnesyltransferases (Hancock, 2003). There are approximately 300 proteins with the CAAX motif that are potentially farnesylated. To investigate pRb's effects on these proteins, we analyzed AC61 cells or MEFs metabolically labeled with [^{3}H]farnesol. In 10% FBS, pRb-negative cells showed an increased density of farnesylated protein bands. When serum was depleted, this difference became greater (Figure 6F; Figure S13). These findings suggest that *Rb* loss induces enhanced global protein farnesylation.

Clinical Relevance of the pRb-N-Ras Pathway in Medullary Thyroid Carcinomas

Human medullary thyroid carcinomas (MTCs) are pathologically similar to the C cell adenocarcinomas in the mice analyzed in this study. Human C cell adenoma is extremely rare. Familial MTCs are frequently associated with mutation in the *ret* oncogene; however, almost half of sporadic MTCs are free of the *ret* mutation (Marsh et al., 2003), indicating a *ret*-independent mechanism involved in human C cell carcinogenesis. To address the relevance of the pRb-N-Ras pathway in human tumors, we

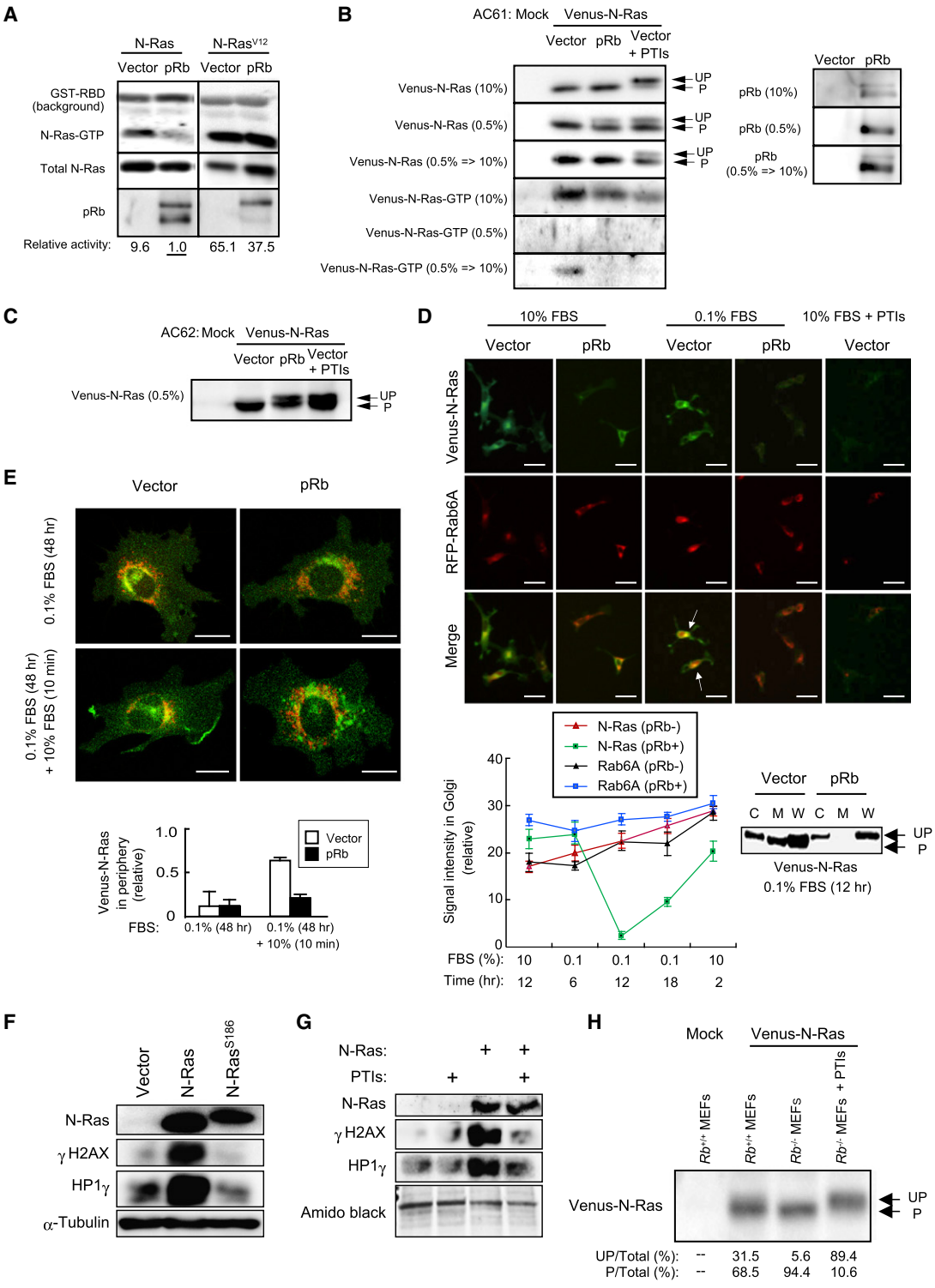

Figure 5. Effects of pRb on N-Ras Isoprenylation and Membrane Trafficking

(A) AC61 cells transfected with 0.25 μg pBabe-puro-N-Ras or pBabe-puro-N-Ras^{V12} together with 2.5 μg pSG5 or pSG5L-HA-Rb were selected and analyzed for GTP-bound N-Ras or status of the indicated proteins in the presence of 10% FBS. Pull-down of GTP-loaded N-Ras was performed using glutathione S-transferase (GST)-fused Ras-binding domain (RBD) of Raf. N-Ras-GTP:total ratio in the presence of N-Ras and pRb (lane 2) was set to 1.0, and relative N-Ras activity in other lanes was estimated.

(B) AC61 cells infected with pLXSB or pLXSB-Rb and selected were transiently transfected with pCAGGS-Venus^{A207R}-N-Ras, treated under the indicated conditions, and analyzed for N-Ras prenylation status (top three rows) and activity (bottom three rows). PTIs = mixture of prenyltransferase inhibitors (FTI-II and FTI-277

analyzed 13 sporadic MTC cases, of which 6 (46%) were immunohistochemically negative for pRb and 7 (54%) were negative for N-Ras (Figure 7A). Notably, 6 of 7 N-Ras-negative tumors were negative for pRb (Figure 7B). This finding in human sporadic MTC is consistent with the requirement of N-Ras suppression in *Rb*-deficient C cell carcinogenesis in mice.

DISCUSSION

The current work provides evidence that in the absence of pRb, E2F-1 and E2F-3 participate in the transactivation of most of the genes involved in protein isoprenylation either directly or via SREBPs. This at least partially explains the Ras activity elevation induced by pRb inactivation (Figure S14A). It would be of interest to ascertain whether under physiological conditions, Ras and pRb activities oscillate due to mutual suppression via cyclin D/Cdk4/6 and E2F/isoprenylation (Figure S14B). Furthermore, this study partially clarifies the mechanism of the tumor suppressor function of wild-type Ras. It has previously been shown that loss of the normal *ras* allele, in addition to activating mutation, is required for tumorigenesis (see references in Zhang et al., 2001). This study indicates that N-Ras and N-Ras^{V12} exert different functions in *Rb*-deficient cells where only N-Ras can induce p130-dependent cellular senescence, which explains why N-Ras^{V12} requires pRb to induce cellular senescence.

Cell-cycle-dependent Ras activation was noted by Taylor and Shalloway (1996). Later, it was determined that pRb inactivation (Raptis et al., 1997) or genetic loss (Lee et al., 1999) elevates Ras activity. The latter study observed that high N-Ras activation was sharply induced in serum-starved $Rb^{-/-}$ MEFs only 10 min after serum restimulation. We suspect that during serum starvation, pRb-negative cells pool greater numbers of N-Ras-GDP molecules in the space where GDP to GTP exchange readily occurs upon serum restimulation. Indeed, our results suggest that isoprenylated Ras-GDP proteins are aberrantly enriched in the Golgi complex in pRb-negative cells during serum starvation. At Golgi, Ras is activated through Src-mediated activation of phospholipase Cγ. The nature of Ras signaling generated from Golgi is supposed to be distinct from that generated from the plasma membrane in terms of activation of JNK, ERK, AKT, and Ral pathways (Hancock, 2003; Quatela and Philips, 2006). Therefore, in addition to moderate-level activation, enrichment of N-Ras in Golgi in *Rb*-deficient cells may assign a specific role to itself.

Simultaneous *N-ras* or *K-ras* deletion rescues differentiation defects in *Rb* null embryos and prolongs life span with no detectable impact on E2F-dependent ectopic proliferation and apoptosis (Takahashi et al., 2003, 2004). This is in line with our observation that the isoprenylation-dependent regulation of Ras activation is genetically downstream of E2Fs in the absence of pRb (Figure S14A). The limited effect of E2F deletion on differentiation defects in $Rb^{-/-}$ embryos can be explained by the redundant functions shared by E2F family members. Indeed, deletion of individual E2Fs in $Rb^{-/-}$ embryos results in varying degrees of rescue of erythropoiesis (Wikenheiser-Brokamp, 2006; Dirlam et al., 2007). The extended life span of *Rb*-deficient embryos achieved by additionally deleting *N-ras* was apparently due to the rescue of hepatic anemia (Takahashi et al., 2003). Although the etiology of *Rb*-deficient anemia is still controversial, a significant genetic interaction seems to exist between *E2F*s and *N-ras* in *Rb*-mediated erythropoiesis. Furthermore, common C cell tumor phenotypes in $Rb^{+/-}$;$E2F3^{-/-}$ and $Rb^{+/-}$;$N\text{-}ras^{-/-}$ mice, the senescence-inducing activity of E2F-3 in vivo (Lazzerini Denchi et al., 2005), and the role of E2F-3 in regulating the transcription of genes involved in Ras isoprenylation (this study) suggest that *E2F3* and *N-ras* are genetically linked in *Rb*-deficient C cell carcinogenesis.

Our observation of less frequent senescence markers, compared to DDR, in early *Rb*-deficient adenomas indicates that DDR chronologically precedes the appearance of senescence markers during adenoma formation. However, this does not necessarily mean that *Rb* loss-induced DNA damage is a prerequisite for inducing cellular senescence. To further address this issue, we are analyzing $Rb^{+/-}$;$ATM^{-/-}$ mice (A.S. and C.T., unpublished data). The RB pathway has been linked to DDR through E2F-dependent pathways (Pickering and Kowalik, 2006) involving cyclin E (Tort et al., 2006) or Mad2 (Hernando et al., 2004). Our study proposes that N-Ras or other isoprenylated proteins may participate in accumulating DNA double-strand breaks in *Rb*-deficient cells.

This study also elucidates the tumor suppressor roles of p130, p16^{Ink4a}, Arf, and Suv39h1 in the absence of pRb. Despite the role of p53 in human retinoblastoma, $Rb^{+/-}$;$p53^{+/-}$ mice generate C cell adenocarcinoma at a lower frequency (8%) following spontaneous mutation in the *ret* oncogene (Coxon et al., 1998) compared to $Rb^{+/-}$;$N\text{-}ras^{-/-}$ mice (91.6%). This

at 10 μM and GGTI-298 at 2 μM). Unprenylated (UP) and prenylated (P) Venus-N-Ras proteins are indicated by arrows. The status of transduced pRb in each condition is indicated at right.

(C) Another *Rb*-deficient $N\text{-}ras^{-/-}$ C cell tumor line, AC62, was analyzed in 0.5% FBS as in (B).

(D) Top: AC61 cells prepared as in (B) and cotransfected with pCAGGS-Venus^{A207R}-N-Ras (green) and pCXN2-RFP-Rab6A (red) were monitored using fluorescence microscopy under the indicated conditions. Scale bars = 40 μm. Merged signals (arrows) are shown. Bottom left: relative intensity of signals in Golgi (RFP-Rab6A-positive area) was measured using NIH ImageJ 1.4 and quantified at the indicated time points. Results show mean ± SEM from 90 cells observed in three experiments. Bottom right: cells cultured in 0.1% FBS for 12 hr were lysed and fractionated. C, cytosolic; M, membranous; W, whole-cell lysates.

(E) Top: AC61 cells were cotransfected with 0.25 μg pCAGGS-Venus^{A207R}-N-Ras (green) and 0.25 μg pCXN2-RFP-Rab6A (red) together with 2.5 μg pCMV or pCMV-Rb. Cells were grown in 10% FBS for 24 hr, serum starved in 0.1% FBS for an additional 48 hr, restimulated with 10% FBS, and analyzed at the indicated time points using a laser confocal fluorescence microscope. Scale bars = 10 μm. Bottom: signal intensity of Venus-N-Ras in the cell periphery was measured using NIH ImageJ 1.4 and quantified from observation of 50 cells each. Bars show mean + SEM from three experiments.

(F) AC61 cells were transfected with pBabe-puro, pBabe-puro-N-Ras, or pBabe-puro-N-Ras^{S186}; selected; and analyzed after 12 days.

(G) AC61 cells were transfected with pBabe-puro or pBabe-puro-N-Ras; selected; treated with 2.5 μM FTI-II, 2.5 μM FTI-277, and 0.5 μM GGTI-298 (PTIs) or with vehicle (DMSO); and analyzed as in (F). Amido black stain is shown as a loading control.

(H) Paired MEFs of the indicated genotypes were transfected with Venus-N-Ras for 8 hr, grown under 0.5% FBS for 24 hr or treated with PTIs as in (G), and analyzed. Prenylated and unprenylated fractions of total Venus-N-Ras are quantified below. Another pair of MEFs is shown in Figure S8.

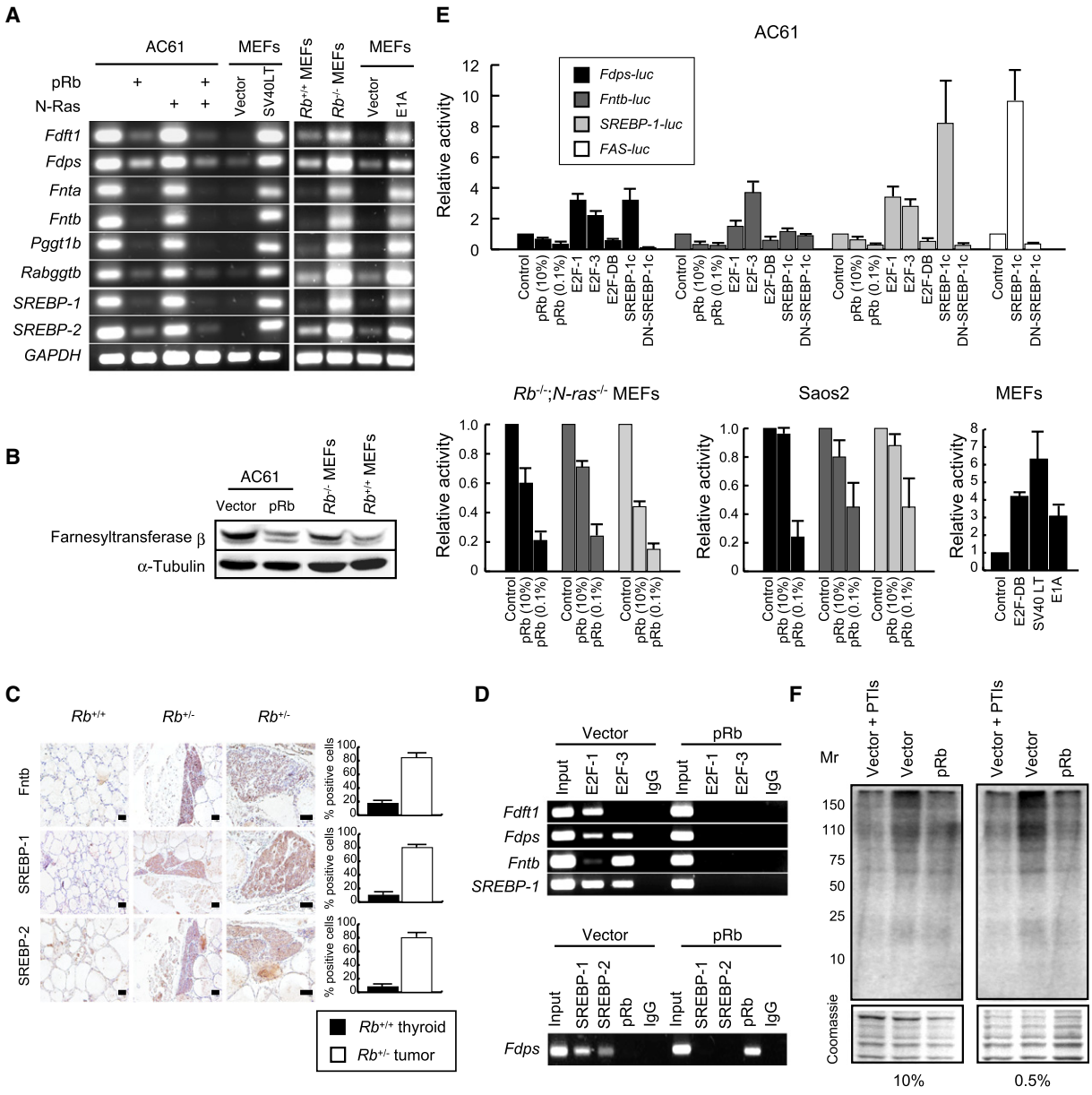

Figure 6. E2F-Dependent Transcriptional Control of Enzymes Involved in Protein Isoprenylation

(A) RT-PCR of the indicated genes in AC61 cells infected with pLXSB or pLXSB-Rb and pBabe-puro or pBabe-puro-N-Ras in the indicated combinations and selected; MEFs infected with pBabe-neo-TAg or control vector; $Rb^{+/+}$ and $Rb^{-/-}$ MEFs cultured in 0.1% FBS for 24 hr; or MEFs infected with pBabe-hygro-E1A or vector control and selected. SV40LT, simian virus 40 large T antigen; E1A, adenovirus E1A.

(B) IB of farnesyltransferase β in AC61 cells expressing the indicated protein and in $Rb^{-/-}$ and $Rb^{+/+}$ MEFs.

(C) IHC analysis of wild-type thyroids and *Rb*-deficient C cell adenomas. Scale bars = 100 μm. Quantification at right was performed as in Figure 1B.

(D) ChIP assay of the indicated gene promoters in AC61 cells infected with pLXSB or pLXSB-Rb. Positions and sequences of the primers in the mouse genome are shown in Figure S11 and Table S4.

(E) Luciferase activity in the indicated cell types transfected with pGL3 containing the indicated luciferase reporters together with pCMV-β-gal and the expression vectors pSG5L-HA-Rb, pcDNA3-HA-E2F-1, pcDNA3-HA-E2F-3, pBabe-puro-E2F-DB, pSV-Sport-SREBP-1c, pSV-Sport dominant-negative (DN)-SREBP-1c, pBabe-neo-Tag, or pBabe-hygro-E1A. Empty vectors (control) were used under the same conditions; results are normalized to β-gal activity and shown as controls set to 1.0. Bars show mean + SEM ($n \geq 3$).

(F) Visualization of [^{3}H]farnesylated proteins in AC61 cells prepared as in (D) and treated under the indicated conditions. Coomassie staining is shown as a loading control.

suggests that, particularly in C cells, the lower p53 activity acts independently to increase genomic instability rather than intimately cooperating with the RB pathway.

Our study also explains the tumor-promoting function of wild-type Ras observed in *Rb*-deficient pituitary glands (Takahashi et al., 2004, 2006) and immortalized fibroblasts (Raptis et al.,

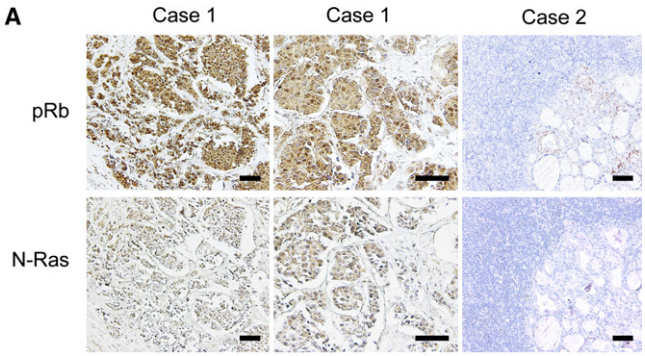

B

	N-Ras	
pRB	Positive	Negative
Positive	6	1
Negative	0	6

p = 0.001998

Figure 7. Analysis of Human Sporadic Medullary Thyroid Carcinomas

(A) IHC analysis of human sporadic medullary thyroid carcinomas (MTCs). Of 13 cases analyzed, representative cases are shown. Scale bars = 100 μm. (B) Chi-square analysis (Fisher's exact test) showing the correlation between pRB and N-Ras expression in 13 sporadic human MTCs. p = 0.001998; $\chi^2 = 9.55$.

1997; Fotiadou et al., 2007). Oncogene-induced cellular senescence is known to occur in limited cell types, but activated Ras promotes carcinogenesis in many cell types. Furthermore, not only Ras but also other isoprenylated proteins including many small GTPase proteins, CENP-E, and CENP-F (Maurer-Stroh et al., 2003) may be orchestrated by pRB via E2Fs. We have previously detected upregulated RhoA, Rac, and Cdc42 activity in *Rb*-deficient cells (Takahashi et al., 2006). Finally, we emphasize that our study provides a rational basis for applying PTIs to pRB-inactivated tumors without somatic *ras* mutations such as retinoblastomas, osteosarcomas, and small cell lung carcinomas.

EXPERIMENTAL PROCEDURES

Animals

$Rb^{+/-}$ mice with various *N-ras* genotypes were described previously (Takahashi et al., 2006). $Rb^{+/-}$ mice were crossed with $Ink4a^{-/-}$, $Arf^{-/-}$, $Ink4a^{-/-}$; $Arf^{-/-}$, or $Suv39h1^{-/-}$ mice, and the resultant progeny were intercrossed to generate mice used in this study. Average age at examination (AE) was determined irrespective of mouse status. Mouse genotyping is described in the Supplemental Experimental Procedures. The protocol of this study was approved by the ethical committee of Kyoto University Graduate School of Medicine, and animals were handled in accordance with the guidelines of Kyoto University.

Cell Culture

Primary C cell adenocarcinoma cell lines were established as described previously (Takahashi et al., 2006), with minor modifications. MEFs were prepared from E12.5 embryos derived by intercrossing $Rb^{+/-}$;*N-ras*$^{+/-}$ or $Rb^{+/-}$;$Ink4a^{+/-}$ mice.

Comet Assay

CometAssay reagent kit was purchased from Trevigen (4250-050-K).

RNA Interference

MISSION TRC shRNA target sets (TRCN 71271 and 71274 for p130; 34391, 34392, and 34393 for N-Ras) and TurboGFP shRNA control vector (SHC004) were purchased from Sigma-Aldrich.

BrdU incorporation

BrdU incorporation was measured as described previously (Takahashi et al., 2004).

Colony Formation Assays

Colony formation was assessed by plating 1×10^3 cells per 60 mm dish. After 14 days cultivation, Giemsa staining was used to visualize colonies. Suppression of colony formation was observed by transfecting 1×10^5 MEFs with 0.5 μg pLXSB and 5 μg pBabe-puro expressing the indicated proteins, followed by 14 days cultivation with 8 μg/ml blasticidin S.

Ras Activation Assay

Pull-down assay to measure N-Ras activity was performed as described previously (Lee et al., 1999).

Prenylation Assay

Cells transiently transfected with pCAGGS-Venus^{A207R}-N-Ras were lysed as described previously (Miki et al., 2007), sonicated for three cycles of 15 s each, and separated on 8%–10% acrylamide SDS-PAGE gel at a low constant voltage (less than 40V for longer than 36 hr). FTI-I (#344150), FTI-277 (#344555), and GGTI-298 (#345883) were purchased from Calbiochem.

RT-PCR

Total RNA was extracted using a QIAGEN RNeasy Mini Kit (74104), and RT-PCR was performed using a TaKaRa RNA PCR Kit (RR019A) and the sequence-specific primers indicated in Table S3.

Chromatin Immunoprecipitation

ChIP reagents (SC-45000, 45001, 45002, and 45003) were purchased from Santa Cruz Biotechnology. Lysates were reacted with specific antibodies for immunoprecipitation. Released DNA was amplified by PCR using the primers indicated in Table S4.

Global Farnesylation Assay

5×10^6 cells were cultured in 10% FBS with 10 mM lovastatin for 4 hr. After lovastatin was removed, the cells were incubated with 1.54 MBq [^{3}H]farnesol in the presence of 10% FBS for 4 hr and then in the presence of 10% or 0.5% FBS for an additional 20 hr. Labeled proteins were analyzed as described previously (Andreas et al., 1999).

Human Tumors

Tumors from patients with sporadic MTC were surgically removed at the Department of Endocrine Surgery and diagnosed at the Department of Pathology, Tokyo Women's Medical University. The protocol of this study was approved by the ethical committee of Tokyo Women's Medical University, and informed consent was obtained from all patients.

ACCESSION NUMBERS

Microarray data described herein have been deposited at the NCBI Gene Expression Omnibus (http://www.ncbi.nlm.nih.gov/geo/) under the accession number GSE12637.

SUPPLEMENTAL DATA

The Supplemental Data include Supplemental Experimental Procedures, Supplemental References, fourteen figures, and four tables and can be found with this article online at http://www.cancercell.org/supplemental/S1535-6108(09)00076-2.

ACKNOWLEDGMENTS

We thank M. Ewen for encouragement and reagents; D. Peeper and T. Taguchi for discussions and reagents; T. Noda and Y. Saiki for critical reading of the manuscript; A. Iwama, T. Jacks, T. Jenuwein, T. Kamijo, R. Kucherlapati, M. Serrano, N. Sharpless, and M. Taketo for animals; S. Gaubatz, W. Hahn, M. Madiredjo, M. Matsuda, W. Sellers, and B. Spiegelman for reagents; H. Futami, Y. Murakami, T. Nishikawa, S. Ogawa, and R. Takahashi for help in analyzing tumors; A. Nishimoto and H. Gu for technical assistance; A. Miyazaki for secretarial assistance; and K. Lee for inspiration. This work was supported by a Research Grant from the Princess Takamatsu Cancer Research Fund; the Takeda Science Foundation; and the Ministry of Education, Culture, Sports, Science and Technology (Japan).

Received: August 21, 2008
Revised: December 8, 2008
Accepted: March 2, 2009
Published: April 6, 2009

REFERENCES

Andreas, D.A., Crick, D.C., Finlin, B.S., and Waechter, C.J. (1999). Rapid identification of cycteine-linked isoprenoyl groups by metabolic labeling with [3H]Farnesol and [3H]geranylgeranoil. In Protein Lipidation Protocols, M.H. Gelb, ed. (Totowa, NJ, USA: Humana Press), 107–123.

Ceol, C.J., and Horvitz, H.R. (2001). dpl-1 DP and efl-1 E2F act with lin-35 Rb to antagonize Ras signaling in *C. elegans* vulval development. Mol. Cell *7*, 461–473.

Chen, Z., Trotman, L.C., Shaffer, D., Lin, H.K., Dotan, Z.A., Niki, M., Koutcher, J.A., Scher, H.I., Ludwig, T., Gerald, W., et al. (2005). Crucial role of p53-dependent cellular senescence in suppression of Pten-deficient tumorigenesis. Nature *436*, 725–730.

Collado, M., Blasco, M.A., and Serrano, M. (2007). Cellular senescence in cancer and aging. Cell *130*, 223–233.

Courtois-Cox, S., Genther Williamns, S.M., Reczeke, E.E., Johnson, B.W., McGillicuddy, L.T., Johannessen, C.M., Holsten, P.E., MacCollin, M., and Cichowski, K. (2006). A negative feedback signaling network underlies oncogene-induced senescence. Cancer Cell *10*, 459–472.

Coxon, A.B., Ward, J.M., Geradts, J., Otterson, G.A., Zajac-Kaye, M., and Kaye, F.J. (1998). RET cooperates with RB/p53 inactivation in a somatic multi-step model for murine thyroid cancer. Oncogene *17*, 1625–1628.

Di Micco, R., Fumagalli, M., and di Fagagna, F. (2007). Breaking news: high-speed race ends in arrest–how oncogenes induce senescence. Trends Cell Biol. *17*, 529–536.

Dimri, G.P. (2005). What has senescence got to do with cancer? Cancer Cell *7*, 505–512.

Dirlam, A., Spike, B.T., and Macleod, K.F. (2007). Deregulated E2f-2 underlies cell cycle and maturation defects in retinoblastoma null erythroblasts. Mol. Cell. Biol. *27*, 8713–8728.

Fotiadou, P.P., Takahashi, C., Rajabi, H.N., and Ewen, M.E. (2007). Wild-type NRas and KRas perform distinct functions during transformation. Mol. Cell. Biol. *27*, 6742–6755.

Goud, B., Zahraoui, A., Tavitian, A., and Saraste, J. (1990). Small GTP-binding protein associated with Golgi cisternae. Nature *345*, 553–556.

Hanahan, D., and Weinberg, R.A. (2000). The hallmarks of cancer. Cell *100*, 57–70.

Hancock, J.F. (2003). Ras proteins: different signals from different locations. Nat. Rev. Mol. Cell Biol. *4*, 373–384.

Hernando, E., Nahle, Z., Juan, G., Diaz-Rodriguez, E., Alaminos, M., Hemann, M., Michel, L., Mittal, V., Gerald, W., Benezra, R., et al. (2004). Rb inactivation promotes genomic instability by uncoupling cell cycle progression from mitotic control. Nature *430*, 797–802.

Laurie, N.A., Donovan, S.L., Shih, C.S., Zhang, J., Mills, N., Fuller, C., Teunisse, A., Lam, S., Ramos, Y., Mohan, A., et al. (2006). Inactivation of the p53 pathway in retinoblastoma. Nature *444*, 61–66.

Lazzerini Denchi, E., Attwooll, C., Pasini, D., and Helin, K. (2005). Deregulated E2F activity induces hyperplasia and senescence-like features in the mouse pituitary gland. Mol. Cell. Biol. *25*, 2660–2672.

Lee, K.Y., Ladha, M.H., McMahon, C., and Ewen, M.E. (1999). The retinoblastoma protein is linked to the activation of Ras. Mol. Cell. Biol. *19*, 7724–7732.

Markey, M.P., Bergseid, J., Bosco, E.E., Stengel, K., Xu, H., Mayhew, C.N., Schwemberger, S.J., Braden, W.A., Jiang, Y., Babcock, G.F., et al. (2007). Loss of the retinoblastoma tumor suppressor: differential action on transcriptional programs related to cell cycle control and immune function. Oncogene *26*, 6307–6318.

Marsh, D.J., Theodosopoulos, G., Martin-Schulte, K., Richardson, A.L., Philips, J., Roher, H.D., Delbridge, L., and Robinson, B.G. (2003). Genome-wide copy number imbalances identified in familial and sporadic medullary thyroid carcinoma. J. Clin. Endocrinol. Metab. *88*, 1866–1872.

Maurer-Stroh, S., Washietl, S., and Eisenhaber, F. (2003). Protein prenyltransferases. Genome Biol. *4*, 212.

Miki, T., Takegami, Y., Okawa, K., Muraguchi, T., Noda, M., and Takahashi, C. (2007). The reversion-inducing cysteine-rich protein with Kazal motifs (RECK) interacts with membrane type 1 matrix metalloproteinase and CD13/aminopeptidase N and modulates their endocytic pathways. J. Biol. Chem. *282*, 12341–12352.

Mooi, W.J., and Peeper, D.S. (2006). Oncogene-induced cell senescence–halting on the road to cancer. N. Engl. J. Med. *355*, 1037–1046.

Narita, M., Nunez, S., Heard, E., Narita, M., Lin, A.W., Hearn, S.A., Spector, D.L., Hannon, G.J., and Lowe, S.W. (2003). Rb-mediated heterochromatin formation and silencing of E2F target genes during cellular senescence. Cell *113*, 703–716.

Peeper, D.S., Upton, T.M., Ladha, M.H., Neuman, E., Zalvide, J., Bernards, R., DeCaprio, J.A., and Ewen, M.E. (1997). Ras signalling linked to the cell-cycle machinery by the retinoblastoma protein. Nature *386*, 177–181.

Pickering, M.T., and Kowalik, T.F. (2006). Rb inactivation leads to E2F1-mediated DNA double-strand break accumulation. Oncogene *25*, 746–755.

Quatela, S.E., and Philips, M.R. (2006). Ras signaling on the Golgi. Curr. Opin. Cell Biol. *18*, 162–167.

Raptis, L., Brownell, H.L., Corbley, M.J., Wood, K.W., Wang, D., and Haliotis, T. (1997). Cellular ras gene activity is required for full neoplastic transformation by the large tumor antigen of SV40. Cell Growth Differ. *8*, 891–901.

Rowland, B.D., Denissov, S.G., Douma, S., Stunnenberg, H.G., Bernards, R., and Peeper, D.S. (2002). E2F transcriptional repressor complexes are critical downstream targets of p19(ARF)/p53-induced proliferative arrest. Cancer Cell *2*, 55–65.

Sage, J., Mulligan, G.J., Attardi, L.D., Miller, A., Chen, S., Williams, B., Theodorou, E., and Jacks, T. (2000). Targeted disruption of the three Rb-related genes leads to loss of G(1) control and immortalization. Genes Dev. *14*, 3037–3050.

Sakakura, Y., Shimano, H., Sone, H., Takahashi, A., Inoue, N., Toyoshima, H., Suzuki, S., and Yamada, N. (2001). Sterol regulatory element-binding proteins induce an entire pathway of cholesterol synthesis. Biochem. Biophys. Res. Commun. *286*, 176–183.

Sellers, W.R., Novitch, B.G., Miyake, S., Heith, A., Otterson, G.A., Kaye, F.J., Lassar, A.B., and Kaelin, W.G., Jr. (1998). Stable binding to E2F is not required for the retinoblastoma protein to activate transcription, promote differentiation, and suppress tumor cell growth. Genes Dev. *12*, 95–106.

Shiloh, Y. (2003). ATM and related protein kinases: safeguarding genome integrity. Nat. Rev. Cancer *3*, 155–168.

Szkopinska, A., and Plochocka, D. (2005). Farnesyl diphophate synthase; regulation of product specificity. Acta Biochim. Pol. *52*, 45–55.

Takahashi, C., Bronson, R.T., Socolovsky, M., Contreras, B., Lee, K.Y., Jacks, T., Noda, M., Kucherlapati, R., and Ewen, M.E. (2003). Rb and N-ras function together to control differentiation in the mouse. Mol. Cell. Biol. *23*, 5256–5268.

Takahashi, C., Contreras, B., Bronson, R.T., Loda, M., and Ewen, M.E. (2004). Genetic interaction between Rb and K-ras in the control of differentiation and tumor suppression. Mol. Cell. Biol. *24*, 10406–10415.

Takahashi, C., Contreras, B., Iwanaga, T., Takegami, Y., Bakker, A., Bronson, R.T., Noda, M., Loda, M., Hunt, J.L., and Ewen, M.E. (2006). Nras loss induces

metastatic conversion of Rb1-deficient neuroendocrine thyroid tumor. Nat. Genet. *38*, 118–123.

Taylor, S.J., and Shalloway, D. (1996). Cell cycle-dependent activation of Ras. Curr. Biol. *6*, 1621–1627.

Todaro, G.J., and Green, H. (1963). Quantitative studies of the growth of mouse embryo cells in culture and their development into established lines. J. Cell Biol. *17*, 299–313.

Tomoda, C., Moatamed, F., Naeim, F., Hershman, J.M., and Sugawara, M. (2008). Indomethacin inhibits cell growth of medullary thyroid carcinoma by reducing cell cycle progression into S phase. Exp. Biol. Med. (Maywood) *233*, 1433–1440.

Tort, F., Bartkova, J., Sehested, M., Orntoft, T., Lukas, J., and Bartek, J. (2006). Retinoblastoma pathway defects show differential ability to activate the constitutive DNA damage response in human tumorigenesis. Cancer Res. *66*, 10258–10263.

Tsai, K.Y., MacPherson, D., Rubinson, D.A., Nikitin, A.Y., Bronson, R., Mercer, K.L., Crowley, D., and Jacks, T. (2002). ARF mutation accelerates pituitary tumor development in Rb+/- mice. Proc. Natl. Acad. Sci U S A *99*, 16865–16870.

Wikenheiser-Brokamp, K.A. (2006). Retinoblastoma family proteins: insights gained through genetic manipulation of mice. Cell. Mol. Life Sci. *63*, 767–780.

Young, A.P., Schlisio, S., Minamishima, Y.A., Zhang, Q., Li, L., Grisanzio, C., Signoretti, S., and Kaelin, W.G., Jr. (2008). VHL loss actuates a HIF-independent senescence programme mediated by Rb and p400. Nat. Cell Biol. *10*, 361–369.

Zhang, Z., Wang, Y., Vikis, H.G., Johnson, L., Liu, G., Li, J., Anderson, M.W., Sills, R.C., Hong, H.L., Devereux, T.R., et al. (2001). Wild-type Kras2 can inhibit lung carcinogenesis in mice. Nat. Genet. *29*, 25–33.

Ziebold, U., Lee, E.Y., Bronson, R.T., and Lees, J.A. (2003). E2F3 loss has opposing effects on different pRB-deficient tumors, resulting in suppression of pituitary tumors but metastasis of medullary thyroid carcinomas. Mol. Cell. Biol. *23*, 6542–6552.